

Ionization phase retrieval by angular streaking from random shots of XUV radiationA. S. Kheifets^{1,*}, R. Wielian¹, V. V. Serov², I. A. Ivanov³, A. Li Wang⁴, A. Marinelli⁴ and J. P. Cryan⁴¹*Research School of Physics, The Australian National University, Canberra ACT 2601, Australia*²*General, Theoretical and Computer Physics, Saratov State University, Saratov 410012, Russia*³*Center for Relativistic Laser Science, Institute for Basic Science (IBS), Gwangju 61005, South Korea*⁴*Stanford PULSE Institute, SLAC National Accelerator Laboratory, Menlo Park, California 94025, USA*

(Received 4 March 2022; revised 31 May 2022; accepted 24 August 2022; published 13 September 2022)

We demonstrate an accurate phase retrieval of extreme ultraviolet (XUV) atomic ionization by streaking the photoelectron in a circularly polarized infrared (IR) laser field. Our demonstration is based on a numerical solution of the time-dependent Schrödinger equation. We test this technique using the hydrogen atom ionized by isolated attosecond XUV pulses across a wide range of the photon energies. Importantly, the proposed method works in a random shot mode when the time delay between the ionizing and streaking XUV and IR pulses may vary from shot to shot. This is a significant advantage over the existing interferometric techniques which require a systematic and controllable scan of the XUV and IR delay in one set of measurements. Such a scan may not be possible to take because of the arrival time jitter inherent to the stochastic nature of self-amplified free-electron laser radiation.

DOI: [10.1103/PhysRevA.106.033106](https://doi.org/10.1103/PhysRevA.106.033106)**I. INTRODUCTION**

Angular streaking of extreme ultraviolet (XUV) atomic ionization with a circularly polarized infrared (IR) laser radiation has become a useful tool for characterizing isolated attosecond pulses (IAPs) from free-electron laser (FEL) sources. Initially suggested theoretically [1–4], this method has been implemented in practice for a shot-to-shot characterization of IAP at FEL [5,6]. Angular streaking of XUV ionization (ASXUVI or ASX for brevity) combines elements of the two previously developed techniques: attosecond angular streaking known as the attoclock [7,8] and the attosecond streak camera (ASC) [9–16]. It is analogous to ASC in that XUV pulses are the primary source of ionization while it is common to the attoclock in that the ionized electrons interact with a circularly polarized laser field which rotates the photoelectron momentum distribution (PMD). This rotation is most graphic in the plane perpendicular to the laser propagation direction. The difference with the attoclock is that the latter is a self-referencing technique where both tunneling ionization and steering are driven by the same elliptical IR laser pulse. In its original form [2–6], ASX was considered in an intense IR laser field and analyzed within the strong field approximation (SFA) [17]. An alternative view within the lowest order perturbation theory [18–20] considers IR streaking as an interference phenomenon which opens natural access to the streaking phase Φ_S . The latter is typically decomposed into the XUV ionization (or Wigner) phase and the laser-induced [or continuum-continuum (CC)] phase. These two phases can be converted to the corresponding time-delay components, which add up to the atomic time delay τ_a . This delay is often

interpreted as the time it takes for the electron to be photoionized plus the time it takes for the measurement process to occur. This timing analysis has been used to determine the attosecond time delay in photoemission from atoms [21] and solid surfaces [22]. The latter seminal works opened up the rapidly growing field of attosecond chronoscopy of photoemission [23–25].

A straightforward extension of time-resolved ionization studies to novel FEL sources of XUV radiation is not possible at present. The existing interferometric techniques rely on a systematic and controllable scan of the XUV and IR pulse delay in one set of measurements. The stochastic nature of self-amplified FEL radiation and the inherent timing jitter do not permit such a scan. In the meantime, ASX allows for the retrieval of the XUV ionization phase and the associated timing information from a series of XUV shots arriving at the target atom randomly. In this paper, we demonstrate this useful phase retrieval capability of ASX over a wide range of photoelectron energies right from the ionization threshold and exceeding it many times. We demonstrate the accuracy of the proposed technique by considering the hydrogen atom driven by a femtosecond XUV pulse across a wide range of carrier frequencies. Our demonstration is based on a numerical solution of the time-dependent Schrödinger equation (TDSE). It is verified through comparison with the well-established RABBITT (reconstruction of attosecond beating by interference of two-photon transitions) technique. Both methods are shown to provide comparable phase and timing information.

II. PHYSICAL INTERPRETATION

An interference character of IR streaking of XUV ionization is illustrated in the left panel of Fig. 1. There are three

*A.Kheifets@anu.edu.au

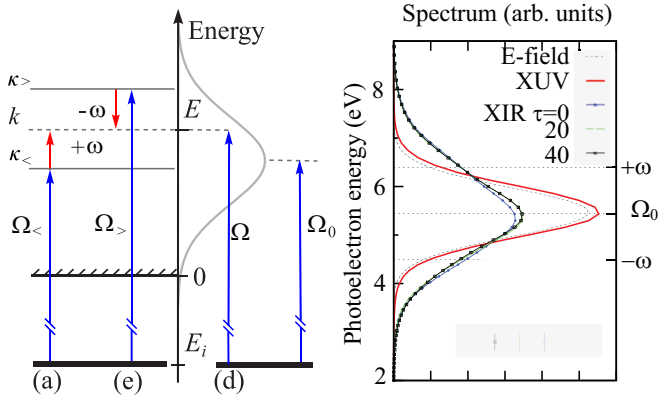


FIG. 1. Left: Schematic representation of IR streaking of XUV ionization. The first order direct process (d) and the second order processes aided by an IR photon absorption (a) and emission (e) are labeled accordingly (adopted from Ref. [19]). Right: Photoelectron spectra of H driven by XUV and XIR are overlapped with the Fourier transform of the electric field.

ionization channels marked (d), (a), and (e), leading to the same final state with the photoelectron energy E . While the direct channel (d) contains an unassisted XUV ionization, two other channels are aided by an IR absorption (a) or emission (e). For these three channels to interfere, the spectral width of the XUV pulse should be large enough to accommodate the $\pm\omega$ laser assisted processes. In the time domain, this means that the XUV pulse is shorter than the laser period. The spectrum of such a pulse is illustrated in the right panel of Fig. 1 and corresponds to ionization of the hydrogen atom at the central XUV and IR photon energies $\Omega_0 = 0.7$ au and $\omega = 0.038$ au, respectively, while the full width at half maximum (FWHM) of the XUV pulse is set to 2 fs. The photoelectron spectrum of an unassisted XUV photoionization [process (d)] is an exact replica of the Fourier transform of the electric E field shifted by the ionization potential. Meanwhile, the photoelectron spectrum of XUV+IR ionization (XIR for brevity) is significantly broadened by the second-order (a) and (e) processes.

The proposed phase retrieval by ASX is based on the following consideration. We apply the SFA and write the photoionization amplitude as [26]

$$b(\mathbf{k}, \tau) = i \int_{t_0}^{\infty} dt E_x(t - \tau) D_x[\mathbf{k} - \mathbf{A}(t)] e^{-i\Phi(t)}. \quad (1)$$

Here the electric field of the XUV pulse E_x is advancing the streaking pulse by the time τ . The streaking field is described by its vector potential

$$\mathbf{A}(t) = A_0 \cos(\omega t) \hat{\mathbf{x}} + A_0 \sin(\omega t) \hat{\mathbf{y}},$$

while the photoelectron momentum is confined to the polarization plane $\mathbf{k} = k \cos \phi \hat{\mathbf{x}} + k \sin \phi \hat{\mathbf{y}}$, where ϕ is the emission angle.

The exponential term contains the so-called Volkov phase,

$$\Phi(t) = \frac{1}{2} \left[\int_t^{\infty} dt' [\mathbf{k} - \mathbf{A}(t')]^2 - k_0^2 t \right], \quad (2)$$

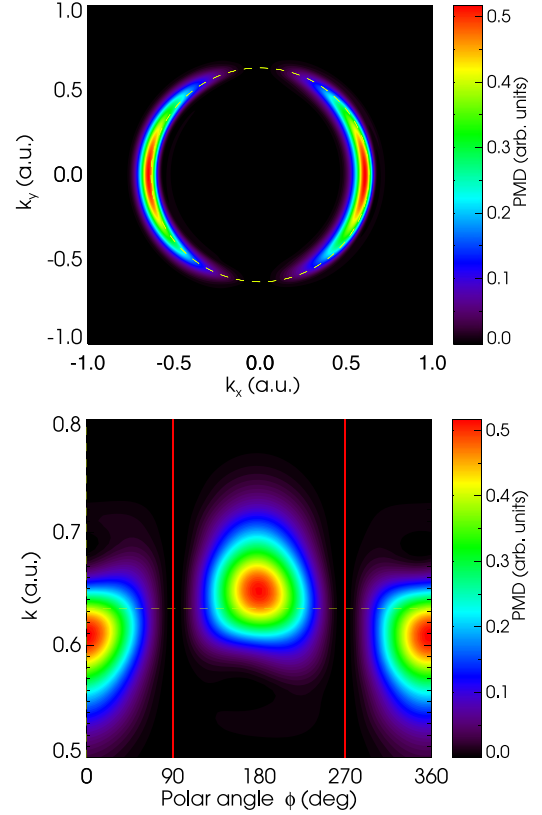


FIG. 2. The PMD of the hydrogen atom in the polarization plane displayed in the Cartesian Cartesian (top) and polar (bottom) coordinates. The dashed circle (top) and the horizontal straight line (bottom) display the momentum value $k_0 = \sqrt{2(\Omega_0 - I_p)}$ from the energy conservation. The solid vertical lines (bottom) define the angular integration limits when calculating the radial momentum profiles $P_{\pm}(k, \tau)$. The XUV and IR time delay $\tau = 0$ in this figure.

in which the photoelectron energy in the absence of streaking $E_0 = k_0^2/2 = \Omega - I_p$. This phase can be estimated by the saddle point method (SPM) which selects the most probable photoelectron trajectories leaving the atom at the time t_{st} and keeping the phase stationary:

$$\Phi'(t_{st}) = \frac{1}{2} |\mathbf{k} - \mathbf{A}(t_{st})|^2 - E_0 = 0. \quad (3)$$

We assume that the XUV pulse is short relative to the IR pulse and shifted relative to its peak position by the time τ . Under these conditions, Eq. (3) is transformed to the following *isochrone* equation [2]:

$$k^2/2 - E_0 = kA_0 \cos(\phi - \omega\tau); \quad \begin{cases} k > k_0 & \phi - \omega\tau \sim 0 \\ k < k_0 & \phi - \omega\tau \sim 180^\circ. \end{cases} \quad (4)$$

Here we neglected the ponderomotive energy $U_p = A_0^2/2$ in a weak streaking field. The bottom panel of Fig. 2 illustrates the isochrone equation (4) most straightforwardly. The PMD extrema, which correspond to $\phi = 0$ and 180° at $\tau = 0$, are displaced relative to the photoelectron momentum k_0 (dashed line) by the amount $\pm A_0$.

In the above derivation, it was implicitly assumed that the phase of the dipole matrix element $D[\mathbf{k} - \mathbf{A}(t)]$ does not

depend on the photoelectron energy. In a more general case, this phase contains an energy-dependent term

$$\arg \{D[\mathbf{k} - \mathbf{A}(t)]\} \propto \alpha |\mathbf{k} - \mathbf{A}(t)|^2/2, \quad (5)$$

where

$$\alpha = \partial \arg D(\sqrt{2E})/\partial E \quad (6)$$

is a generalized definition of the photoelectron group delay in photoemission (see, e.g., Eq. (S10) of Schultze *et al.* [21]). The introduction of this delay modifies the stationary phase equation:

$$\frac{1}{2}|\mathbf{k} - \mathbf{A}(t_{\text{st}})|^2 - E_0 + \frac{\alpha}{2} \frac{d}{dt} [(\mathbf{k} - \mathbf{A}(t_{\text{st}}))^2] = 0. \quad (7)$$

This leads to a modified isochrone equation:

$$\begin{aligned} k^2/2 - E_0 &= kA_0[\cos(\phi - \omega\tau) - \alpha\omega \sin(\phi - \omega\tau)] \\ &\approx kA_0 \cos[\phi - \omega\tau + \omega\alpha]. \end{aligned} \quad (8)$$

In the second line, we used the identity $b \cos x - a \sin x = \sqrt{1 + (ab)^2} \cos(x + y)$, $y = \tan^{-1}(a/b)$ and the long wavelength approximation $\omega\alpha \ll 1$ for the streaking field. Thus the isochrone acquires an additional phase shift $\Phi_S = \omega\alpha$ which can be extracted from the PMD. In the following, we shall demonstrate that $\alpha = \Phi_S/\omega = \tau_a$ under certain XUV and IR pulse parameters. For simplicity of derivation, α was introduced in Eq. (6) solely as the dipole phase derivative. In practice, we will show that it also contains the measurement-induced CC components.

III. NUMERICAL RESULTS

In Fig. 2, we display the PMD of the hydrogen atom ionized with a 2 fs XUV pulse at 6×10^{13} W/cm² and $\Omega_0 = 0.7$ au in the presence of a long IR pulse with $\omega = 0.038$ au ($\lambda = 1200$ nm), FWHM = 25 fs at 1.5×10^{11} W/cm². The XUV pulse is linearly polarized along the \hat{x} axis whereas the IR pulse is circularly polarized in the (xy) plane. The PMD is projected on this plane. The top panel illustrates the dipole angular pattern $\propto \cos^2 \phi$ of the primary XUV ionization of the hydrogen $1s$ initial state which is largely retained in the XIR ionization. The bottom panel shows the polar coordinate representation highlighting the momentum offset induced by the vector potential of the laser pulse. In the exhibited case, the XUV and IR delay $\tau = 0$. To simulate XIR ionization numerically, we run a series of TDSE calculations using the computer code [27]. At each XUV photon energy, we scan the delay between the XUV pulse and the IR laser field (τ) in the range of 0 to 70 au in eight increments.

The modified isochrone equation (8) allows, in principle, for the ASX phase extraction at each pair of the variables k, ϕ . For better clarity, it is more advantageous to conduct such an extraction at the extrema of the PMD. When a limited statistics is available experimentally, the whole lobe of the PMD centered at these extrema can be used. We demonstrate this by integrating the PMD over the $\pm 90^\circ$ angular intervals centered around $\phi = 0$ and $\pm 180^\circ$ (shown by vertical lines in the bottom panel of Fig. 2). We carry out this procedure at several fixed increments of the XUV and IR delay τ . The

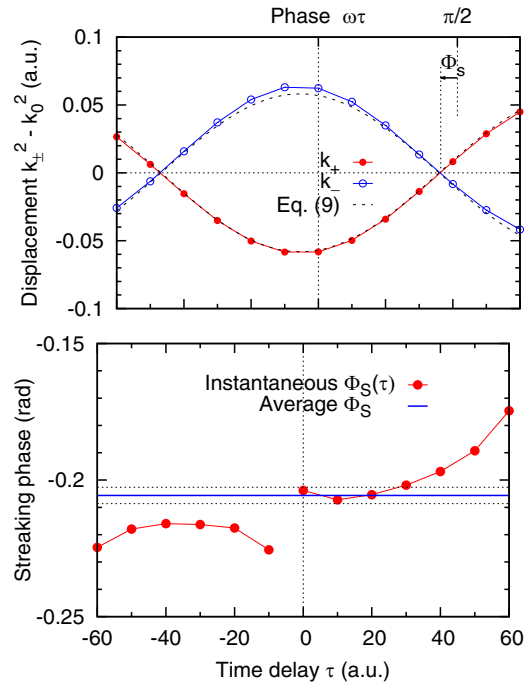


FIG. 3. Top: Radial momentum displacements $k_{\pm}^2/2 - k_0^2/2$ are shown at various XUV and IR delays τ . The dashed line represents the fit with Eq. (9). The arrow indicates the streaking phase Φ_S . Bottom: The fit with Eq. (9) is applied to individual τ values to determine the instantaneous $\Phi_S(\tau)$. The average Φ_S is shown as a solid line with error bars visualized by dotted lines.

corresponding radial momentum profiles $P_{\pm}(k, \tau)$ are shown in the top panel of Fig. 3 for the angular integration range $|\phi| < 90^\circ$. The analogous profiles $P_{-}(k, \tau)$ corresponding to the $|\phi - 180^\circ| < 90^\circ$ integration range mirror closely the set shown in the figure. The two sets of the momentum profiles allow us to determine the mean photoelectron momenta at each τ ,

$$k_{\pm}(\tau) = \int k P_{\pm}(k, \tau) dk / \int P_{\pm}(k, \tau) dk,$$

which are then used to obtain the isochrone phase offset:

$$k_{\pm}^2(\tau)/2 - E_0 = \pm A_0 k_{\pm}(\tau) \cos(\omega\tau + \Phi_S). \quad (9)$$

In our simulation, the ansatz (9) can be applied to the whole set of the time delays τ treating Φ_S as a common fitting parameter. This way an average Φ_S value is obtained as illustrated in the top panel of Fig. 3. Alternatively, we can solve Eq. (9) for each τ value and to obtain an instantaneous $\Phi_S(\tau)$ value. This value would mimic a streaking phase retrieved in a single shot measurement at a given τ . Both sets of streaking phases are shown in the bottom panel of Fig. 3, where the average Φ_S is displayed with the straight solid line while its error bars are exhibited with the dotted lines. While the deviation of $\Phi_S(\tau)$ from Φ_S is exceeding the error bars of the latter, the method works quite satisfactorily even if a single τ determination of the streaking phase is made. The attained accuracy of about 20% is on par with that achieved in other streaking measurements (see, e.g., Ref. [28]).

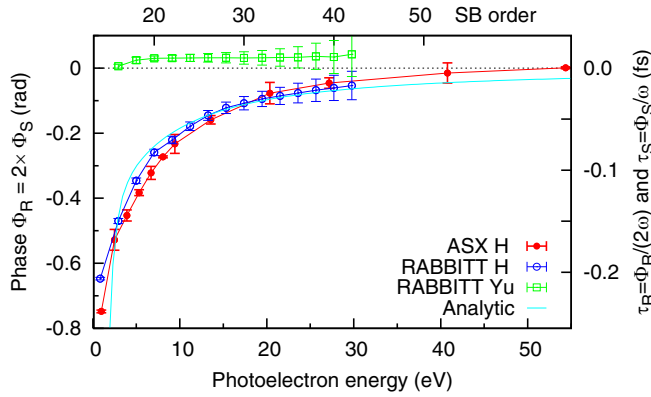


FIG. 4. Left axis: RABBITT phase Φ_R as extracted from Eq. (10) is compared with twice the streaking phase $2\Phi_S$ obtained from the isochrone ansatz Eq. (4). Right axis: RABBITT time delay $\tau_R = \Phi_R/(2\omega)$ and the streaking time delay $\tau_S = \Phi_S/\omega$ are compared with the Coulombic Wigner time delay augmented by the CC correction from Refs. [23,31]. The RABBITT phase and time delay in the Yukawa atom (Yu) are also shown.

We note that Eq. (9) contains the vector potential magnitude which may not be known experimentally because of the laser focus averaging effect. After a sufficient number of XUV shots at random τ is collected, an effective vector potential magnitude can be determined from the maximum vertical displacement between the upward and downward shifted lobes $A_0 = 0.5|k_+ - k_-|_{\max}$ across the whole series. The statistical nature of such a determination will not be detrimental to the accuracy of the phase retrieval, which is rather insensitive to the IR pulse intensity. For instance, at $\Omega = 0.7$ au and the IR pulse intensity of 1.5×10^{11} W/cm², the streaking phase $\Phi_S = -0.196$ rad. This value changes to -0.177 rad at 1.2×10^{11} W/cm² and to -0.211 rad at 1.8×10^{11} W/cm². While these two intensities differ by 50%, the streaking phase Φ_S varies by only 10%. The streaking phase is similarly insensitive to ellipticity. The cited value of $\Phi_S = -0.196$ rad changes only in the fourth significant figure when the circular polarization is reduced to an elliptical one with $\epsilon = 0.9$. At a sufficiently large XUV photon energy, the streaking phase tends to zero as a fast photoelectron is represented by a plane wave. Hence the maximum vertical displacement $2A_0$ is attained at $\tau = 0$. This provides a convenient calibration of the XUV pulse arrival time.

The average streaking phases Φ_S at various XUV photon energies are displayed in Fig. 4. These phases are benchmarked against our present RABBITT calculations on hydrogen at the corresponding XUV energies and the same IR intensity and wavelength. Numerical details of these calculations can be found in preceding works [29,30]. From these simulations, we obtain the RABBITT phase Φ_R by fitting the angular integrated photoelectron spectra at various τ with the following expression:

$$S_{2q}(\tau) = A + B \cos[2\omega\tau - \Phi_R(E)]. \quad (10)$$

Here the sideband index $2q$ defines the photoelectron energy $E = 2q\omega - I_p$. We note that the amplitudes of the RABBITT peaks (10) oscillate with twice the laser frequency $\propto 2\omega\tau$ and the atomic time delay is defined as $\tau_R = \Phi_R/(2\omega)$. In

the meantime, the streaking signal (9) contains the $\propto \omega\tau$ oscillation and we expect the atomic time delay to be expressed as $\tau_S = \Phi_S/\omega$. Therefore, we make a comparison of the RABBITT phase Φ_R with twice the streaking phase $2\Phi_S$. This comparison is shown in Fig. 4. The error bars in the figure indicate the accuracy of the fitting procedure with the isochrone and RABBITT equations (4) and (10), respectively, by employing the Marquardt-Levenberg nonlinear algorithm. We observe a rather close agreement between Φ_R and $2\Phi_S$ in Fig. 4. However, various numerical factors stop us short from claiming these two phases leading to the identical atomic time delays. Such an identity is established in linear streaking and RABBITT [19]. We note that the RABBITT phase Φ_R cannot be determined from Eq. (10) using a single value of τ , as the magnitude coefficients A, B are not known *ab initio* and cannot be determined experimentally. Only the whole set of RABBITT measurements or simulations can be fit by Eq. (10) with a common Φ_R value. Thus, RABBITT is not suitable for a random shot phase determination. In addition, to cover a wide photoelectron energy range of Fig. 4, the large harmonic orders in their 40s should be used in the RABBITT simulations for the hydrogen and Yukawa atoms. This large order leads to progressively increasing error bars in the RABBITT data. We note that the typical harmonic orders in their 20s are employed in most RABBITT experiments. This observation demonstrates another advantage of the proposed scheme which can probe large photoelectron energies without compromising accuracy since the XUV and IR photon energies are entirely decoupled.

The phase of the angular integrated RABBITT signal can be converted to the atomic time delay as $\tau_R = \Phi_R/(2\omega)$. Similarly, the streaking phase can be converted to the time delay as $\tau_S = \Phi_S/\omega$. Both conversions are shown on the right axis of Fig. 4. As the hydrogen atom is free from many-electron correlation and resonances, its atomic time delay is known analytically [23,31]. Comparison of both the ASX and RABBITT time delays with this analytic test is rather accurate across a broad range of XUV energies. As an additional test, we run a set of analogous streaking and RABBITT calculations on the Yukawa atom in which the Coulomb potential is screened as $(Z/r)\exp(-r/a)$, where $Z = 2.785$ and $a = 0.5$, thus maintaining the hydrogen atom ionization potential. Both the streaking and RABBITT phases vanish in the Yukawa atom, thus indicating the Coulomb origin of the atomic time delay in hydrogen. Besides solving the TDSE, we obtain the PMD from the SPM simulations as described in Ref. [32]. The streaking phase vanishes once the same phase extraction method is applied to the SPM data. This provides additional credibility to the proposed technique.

Furthermore, we extended our ASX simulations to a different regime utilizing a mid-IR laser pulse at $\lambda = 10.6 \mu\text{m}$ as in the experiment [5]. The IR intensity was varied between 1.5×10^9 W/cm² and 2.4×10^{10} W/cm² to demonstrate the stability of the streaking phase extraction. Results of these simulations at a fixed XUV photon energy $\Omega = 0.7$ au are shown in Fig. 5. The top panel displays the PMD in the polarization plane at the IR intensity of 2.4×10^{10} W/cm² and the XUV and IR time delay $\tau = 2.5$ fs. The PMD displays both

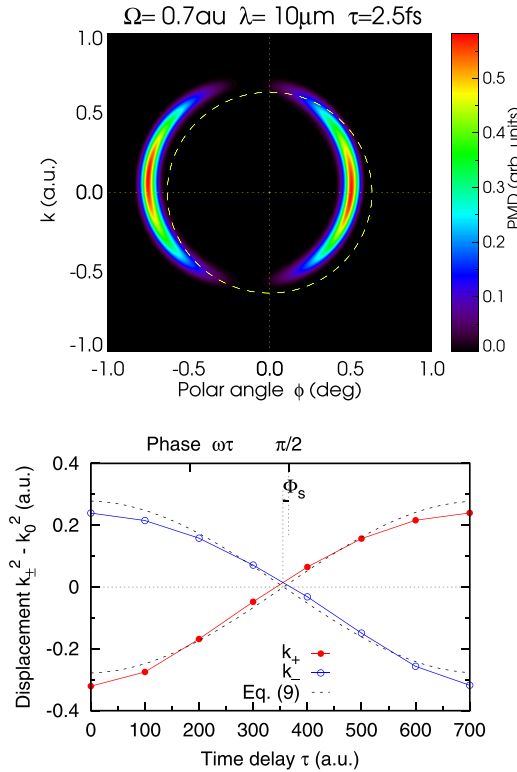


FIG. 5. Top: The PMD of the hydrogen atom in the polarization plane at $\Omega = 0.7$ au, $\lambda = 10.6 \mu\text{m}$, and $\tau = 2.5$ fs is displayed in the Cartesian coordinates. Bottom: Radial momentum displacements $k_{\pm}^2/2 - k_0^2/2$ are shown at various XUV and IR delays τ . The dashed line represents the fit with Eq. (9). The arrow indicates the streaking phase Φ_S .

the radial and angular displacement of the maxima away from XUV polarization direction. With the radial displacements being determined in these maxima directions, the isochrone analysis is shown in the bottom panel of Fig. 5. While the streaking phase is decreased to $\Phi_S = -0.046$ rad, the corresponding time delay grows to $\tau_S = 260$ as. This compares with the time delay value $\tau_S = 125$ as at 1200 nm. Such an increase is expected as the CC correction contains the term

$$\tau_{cc} \propto -\frac{Z}{k^3} \left[\ln 1.16 \frac{k^2}{\omega} - 1 \right], \quad (11)$$

where $k \simeq 0.63$ is the photoelectron momentum and $Z \simeq 1$ the Coulomb charge of the ion remainder [31].

IV. CONCLUSIONS

In conclusion, we demonstrate an accurate retrieval of the streaking phase Φ_S from XUV atomic ionization in the presence of a circularly polarized IR laser field. The rationale of this method is based on the introduction of the streaking phase Φ_S into the isochrone equation (4) derived earlier in Ref. [2] within the SFA. The modified isochrone (8) has two phase shifts. One is due to the XUV and IR delay $\omega\tau$ which can be controlled by an incremented displacement of the short XUV pulse relative to the long IR pulse. An additional term Φ_S is due to the energy-dependent phase of the dipole ioniza-

tion amplitude (6). Our numerical simulations on hydrogen indicate that such an extracted phase can be converted to the atomic time delay $\tau_S = \Phi_S/\omega$, similarly to the analogous conversion of the phase of the RABBITT oscillation $\tau_R = \Phi_R/(2\omega)$. Even though the numerical values of τ_S and τ_R may differ insignificantly in our simulations, their similarity across a wide range of photon energies, right from the ionization threshold, is quite noticeable.

Even though the rationale of the proposed phase extraction is drawn from the SFA, its validity is actually much wider and applies to photoelectrons with the energy as low as only 10% of the ionization potential. Simplicity of the hydrogen atom allows us to test the ASX and RABBITT time delay τ_a against the analytical results [23,31]. These results allow us to interpret the atomic time delay as the time it takes for the electron to be photoionized and the time it takes for the measurement process to occur. This interpretation was challenged recently for Coulombic systems [33] but seems to be confirmed by the present paper. In addition, the proposed technique was extended to the H_2 molecule [34]. Not only did we show an accurate phase extraction, we also reproduced orientation and two-center interference effects which are specific to homonuclear diatomic molecules.

The proposed ASX phase retrieval can be utilized in FEL by collecting a sequence of XUV radiation shots with random arrival times τ . This sequence allows us to determine the effective vector potential magnitude A_0 from the maximum vertical displacement of the two PMD lobes. This determination, conducted at a sufficiently large photoelectron energy, will point to the zero net displacement of the XUV and IR pulses $\tau = 0$. This arrival time calibration along with the known effective A_0 will allow one to conduct the phase determination at the whole set of collected data points. Importantly, the magnitude and phase of the XUV pulse, which may vary from shot to shot, do not affect the proposed phase determination as these parameters do not enter the isochrone equations (4) and (8).

In parallel with the absolute streaking phase determination, one can use a reference of a second ionization state in the same target or ionization from an additional reference target mixed with the original target to determine their relative ionization phase. The reference and target photolines are produced by the same XUV pulse, so they share a common global streaking angle. Their difference in streaking angle will give $\tau_a - \tau_r$, where τ_r is the reference group delay. If we choose a reference photoline that is much higher in energy and has a clear continuum, then τ_r will be negligible. This technique has been implemented and analyzed in the SFA framework [35], where the radial ansatz Eq. (9) can be used to directly read on a single-shot basis.

ACKNOWLEDGMENTS

V.V.S. was supported by the Australian Research Council Discovery Project No. DP190101145. I.A.I. was supported by the Institute for Basic Science under the Grant IBS-R012-D1. J.P.C., A.M., and A.L.W. were supported by the U.S. Department of Energy (DOE), Office of Science, Office of Basic Energy Sciences (BES), Chemical Sciences, Geosciences, and Biosciences Division (CSGB).

- [1] Z. X. Zhao, Z. Chang, X. M. Tong, and C. D. Lin, Circularly-polarized laser-assisted photoionization spectra of argon for attosecond pulse measurements, *Opt. Express* **13** (6), 1966 (2005).
- [2] A. K. Kazansky, A. V. Bozhevolnov, I. P. Sazhina, and N. M. Kabachnik, Interference effects in angular streaking with a rotating terahertz field, *Phys. Rev. A* **93**, 013407 (2016).
- [3] S. Li, Z. Guo, R. N. Coffee, K. Hegazy, Z. Huang, A. Natan, T. Osipov, D. Ray, A. Marinelli, and J. P. Cryan, Characterizing isolated attosecond pulses with angular streaking, *Opt. Express* **26** (4), 4531 (2018).
- [4] A. K. Kazansky, I. P. Sazhina, and N. M. Kabachnik, Fast retrieval of temporal characteristics of FEL pulses using streaking by THz field, *Opt. Express* **27** (9), 12939 (2019).
- [5] N. Hartmann, G. Hartmann, R. Heider, M. S. Wagner, M. Ilchen, J. Buck, A. O. Lindahl, C. Benko, J. Grünert, J. Krzywinski *et al.*, Attosecond time-energy structure of x-ray free-electron laser pulses, *Nat. Photonics* **12**, 215 (2018).
- [6] J. Duris, S. Li, T. Driver, E. G. Champenois, J. P. MacArthur, A. A. Lutman, Z. Zhang, P. Rosenberger, J. W. Aldrich, R. Coffee *et al.*, Tunable isolated attosecond x-ray pulses with gigawatt peak power from a free-electron laser, *Nat. Photonics* **14**, 30 (2020).
- [7] P. Eckle, M. Smolarski, P. Schlup, J. Biegert, A. Staudte, M. Schoffler, H. G. Muller, R. Dorner, and U. Keller, Attosecond angular streaking, *Nat. Phys.* **4**, 565 (2008).
- [8] A. N. Pfeiffer, C. Cirelli, M. Smolarski, D. Dimitrovski, M. Abu-samaha, L. B. Madsen, and U. Keller, Attoclock reveals natural coordinates of the laser-induced tunnelling current flow in atoms, *Nat. Phys.* **8**, 76 (2012).
- [9] E. Constant, V. D. Taranukhin, A. Stolow, and P. B. Corkum, Methods for the measurement of the duration of high-harmonic pulses, *Phys. Rev. A* **56**, 3870 (1997).
- [10] J. Itatani, F. Quéré, G. L. Yudin, M. Y. Ivanov, F. Krausz, and P. B. Corkum, Attosecond Streak Camera, *Phys. Rev. Lett.* **88**, 173903 (2002).
- [11] E. Goulielmakis, M. Uiberacker, R. Kienberger, A. Baltuska, V. Yakovlev, A. Scrinzi, T. Westerwalbesloh, U. Kleineberg, U. Heinzmann, M. Drescher *et al.*, Direct measurement of light waves, *Science* **305** (5688), 1267 (2004).
- [12] R. Kienberger, E. Goulielmakis, M. Uiberacker, A. Baltuska, V. Yakovlev, F. Bammer, A. Scrinzi, T. Westerwalbesloh, U. Kleineberg, U. Heinzmann *et al.*, Atomic transient recorder, *Nature (London)* **427**, 817 (2004).
- [13] V. S. Yakovlev, F. Bammer, and A. Scrinzi, Attosecond streaking measurements, *J. Mod. Opt.* **52** (2-3), 395 (2005).
- [14] U. Fröhling, M. Wieland, M. Gensch, T. Gebert, B. Schütte, M. Krikunova, R. Kalms, F. Budzyn, O. Grimm, J. Rossbach *et al.*, Single-shot terahertz-field-driven x-ray streak camera, *Nat. Photonics* **3**, 523 (2009).
- [15] C.-H. Zhang and U. Thumm, Streaking and Wigner time delays in photoemission from atoms and surfaces, *Phys. Rev. A* **84**, 033401 (2011).
- [16] M. Ivanov and O. Smirnova, How Accurate is the Attosecond Streak Camera? *Phys. Rev. Lett.* **107**, 213605 (2011).
- [17] X. Zhao, S. Li, T. Driver, V.-H. Hoang, A.-T. Le, J. P. Cryan, A. Marinelli, and C. D. Lin, Characterization of single-shot attosecond pulses with angular streaking photoelectron spectra, *Phys. Rev. A* **105**, 013111 (2022).
- [18] J. M. Dahlström, A. L. Huillier, and A. Maquet, Introduction to attosecond delays in photoionization, *J. Phys. B: At. Mol. Opt. Phys.* **45** (18), 183001 (2012).
- [19] J. M. Dahlström, D. Guénot, K. Klünder, M. Gisselbrecht, J. Mauritsson, A. L. Huillier, A. Maquet, and R. Taïeb, Theory of attosecond delays in laser-assisted photoionization, *Chem. Phys.* **414**, 53 (2013).
- [20] A. Maquet, J. Caillat, and R. Taïeb, Attosecond delays in photoionization: Time and quantum mechanics, *J. Phys. B: At. Mol. Opt. Phys.* **47** (20), 204004 (2014).
- [21] M. Schultze, M. Fiess, N. Karpowicz, J. Gagnon, M. Korbman, M. Hofstetter, S. Neppl, A. L. Cavalieri, Y. Komninos, T. Mercouris *et al.*, Delay in Photoemission, *Science* **328** (5986), 1658 (2010).
- [22] A. L. Cavalieri, N. Müller, T. Uphues, V. S. Yakovlev, A. Baltuska, B. Horvath, B. Schmidt, L. Blümel, R. Holzwarth, S. Hendel *et al.*, Attosecond spectroscopy in condensed matter, *Nature (London)* **449**, 1029 (2007).
- [23] R. Pazourek, S. Nagele, and J. Burgdorfer, Time-resolved photoemission on the attosecond scale: opportunities and challenges, *Faraday Discuss.* **163**, 353 (2013).
- [24] R. Pazourek, S. Nagele, and J. Burgdorfer, Attosecond chronoscopy of photoemission, *Rev. Mod. Phys.* **87**, 765 (2015).
- [25] U. Thumm, Q. Liao, E. M. Bothschafter, F. Süßmann, M. F. Kling, and R. Kienberger, Attosecond physics: Attosecond streaking spectroscopy of atoms and solids, in *Photonics*, edited by D. L. Andrews (John Wiley & Sons, Ltd., 2015), Chap. 13, pp. 387–441.
- [26] M. Kitzler, N. Milosevic, A. Scrinzi, F. Krausz, and T. Brabec, Quantum Theory of Attosecond XUV Pulse Measurement by Laser Dressed Photoionization, *Phys. Rev. Lett.* **88**, 173904 (2002).
- [27] V. V. Serov, Calculation of intermediate-energy electron-impact ionization of molecular hydrogen and nitrogen using the paraxial approximation, *Phys. Rev. A* **84**, 062701 (2011).
- [28] G. Schmid, K. Schnorr, S. Augustin, S. Meister, H. Lindenblatt, F. Trost, Y. Liu, N. Stojanovic, A. Al-Shemmary, T. Golz *et al.*, Terahertz-Field-Induced Time Shifts in Atomic Photoemission, *Phys. Rev. Lett.* **122**, 073001 (2019).
- [29] A. W. Bray, F. Naseem, and A. S. Kheifets, Simulation of angular-resolved RABBITT measurements in noble-gas atoms, *Phys. Rev. A* **97**, 063404 (2018).
- [30] A. S. Kheifets, Strongly resonant RABBITT on lithium, *Phys. Rev. A* **104**, L021103 (2021).
- [31] V. V. Serov, V. L. Derbov, and T. A. Sergeeva, Interpretation of the time delay in the ionization of Coulomb systems by attosecond laser pulses, in *Advanced Lasers*, Springer Series in Optical Sciences, Vol. 193 (Springer, Berlin, 2015), pp. 213–230.
- [32] A. S. Kheifets, J. Cesca, V. V. Serov, K. T. Kim, and I. A. Ivanov, Two-pulse interference and correlation in an attoclock, *Phys. Rev. A* **104**, 033118 (2021).
- [33] U. Saalman and J. M. Rost, Proper Time Delays Measured by Optical Streaking, *Phys. Rev. Lett.* **125**, 113202 (2020).
- [34] V. V. Serov and A. S. Kheifets, XUV ionization of the H₂ molecule studied with attosecond angular streaking, [arXiv:2204.09161](https://arxiv.org/abs/2204.09161).
- [35] T. D. Driver *et al.*, Isolated, tunable soft x-ray attosecond pulses at μj pulse energy from a free-electron laser, in *7th International Conference on Attosecond Science and Technology* (University of Szeged, Hungary, 2019).